Journal of Oceanography, Vol. 58, pp. 565 to 575, 2002

Steady Response of a Ventilated Thermocline to Enhanced Ekman Pumping

Atsushi Kubokawa* and Shang-Ping Xie†

Graduate School of Environmental Earth Science, Hokkaido University, Sapporo 060-0810, Japan

(Received 2 July 2001; in revised form 4 December 2001; accepted 6 December 2001)

The steady response of the ventilated thermocline to an increase in Ekman pumping is investigated, focusing on the effect of the mixed layer depth distribution on the subsurface density anomaly. We consider only the subtropical gyre, and the mixed layer is assumed to be deep in the northwest and shallow elsewhere with a narrow transition zone separating the deep and shallow mixed layer regions. At the intersection of this narrow transition zone and the outcrop line, low potential vorticity fluid is subducted into and ventilates the thermocline. In such a situation, an enhancement of the Ekman pumping confined to the northern subtropical gyre leads to pronounced subsurface cold anomalies in the southern subtropics, which is free of anomalous forcing. These density anomalies are much greater than those that occur when either the mixed layer depth is zonally uniform or the Ekman pumping is enhanced in the whole subtropical gyre. They are caused by anomalous changes in the trajectory of the low potential vorticity fluid in response to anomalous Sverdrup flow.

Keywords:
· Oceanic response,
· intensification of westerlies,
· mixed layer depth front,
· subsurface temperature anomaly,
· ventilated thermocline model.

1. Introduction

Recent climate studies have shown that westerly winds over the North Pacific Ocean change on decadal and/or interdecadal time scales, causing changes in the ocean thermocline (Deser *et al*., 1996; Yasuda and Hanawa, 1997). A recent event is the intensification of westerly winds in the mid-1970s, and Deser *et al*. (1996) observed subsurface cold anomalies after this event, which subsequently spread southwestward in the thermocline.

A change in surface wind can affect subsurface ocean temperatures by two mechanisms. First it changes sea surface temperatures (SST) through changes in surface sensible and latent heat flux and in meridional heat transport by surface Ekman flow. Through subduction processes, these SST anomalies give rise to temperature anomalies in the main thermocline. The second mechanism for wind-induced subsurface temperature changes is through Ekman pumping. Hereafter, we will call the former mechanism SST forcing and the latter w_e forcing for the sake of discussion. The thermocline response to SST and w_e forcings is believed to be very different: subsurface temperature anomalies induced by SST anomalies spread in a southwestward direction along isopycnal streamlines within the main thermocline, whereas those induced by w_e anomalies take the form of the first baroclinic Rossby wave propagating mainly westward (Liu, 1999; Huang and Pedlosky, 1999). Because of this difference in response characteristics between the two forcing mechanisms, the southwestward spreading of cold subsurface temperature anomalies observed after the mid-1970s wind shift over the North Pacific (Deser *et al*., 1996; Yasuda and Hanawa, 1997) is generally attributed to the SST forcing (Schneider *et al*., 1999; Nonaka *et al*., 2000).

However, a recent ocean general circulation model experiment (GCM) suggests that the w_e-induced thermocline response might look quite similar to the SST-forced one. In response to an intensification of westerly wind stress localized to the northern subtropical gyre, Inui *et al*. (1999) reported a subsurface cooling that extends southwestward, much as is observed in the North Pacific after the mid-1970s. In either a linear reduced-gravity model or the original LPS ventilated thermocline model (Luyten *et al*., 1983) with zonally uniform distributions of surface density, the increased Ekman pumping (due to the intensified westerlies in the Inui *et al*. experiment) will cause a subsurface warming within the latitude band where the Ekman pumping anomalies are applied. Outside the forcing latitudes, these models predict zero response (see Subsection 3.1). This result of Inui *et al*.

* Corresponding author. E-mail: kubok@ees.hokudai.ac.jp

† Present address: IPRC/SOEST and Department of Meteorology, University of Hawaii, 2525 Correa Road, Honolulu, Hawaii 96822, U.S.A.

(1999), in which the pronounced subsurface cooling takes place south of the forcing latitudes, seems contrary to these simple model predictions.

The subsurface density structure is determined by the three-dimensional potential vorticity distribution. Kubokawa and Inui (1999) found that the potential vorticity of ventilated fluid in an ocean GCM is strongly affected by the distribution of mixed layer depth (MLD). In ocean GCMs, the mixed layer tends to be deep in the northwest and shallow in the southeast of the subtropical gyre, and the transition zone separating the deep and shallow mixed layer is very narrow (see Williams *et al*., 1995; Kubokawa and Inui, 1999). A similar MLD distribution can also be seen in the real ocean (e.g., Huang and Russell, 1994; Suga *et al*., 1997). Kubokawa and Inui (1999) showed that the intersection of this narrow transition zone of the MLD and the outcrop line is a source of low potential vorticity (PV) fluid in an ocean GCM (see also Kubokawa, 1999), although the detailed dynamics determining the MLD distribution is still unclear. Inui *et al*. (1999) linked the subsurface cold anomaly with a change in the path of this low PV fluid, and suggested that the latter results from changes in the MLD distribution and hence in the formation region of the low-PV water. Given that the gyre circulation will change in response to an Ekman pumping anomaly, such a circulation change can also cause the path of the low-PV water to vary. This circulation-induced change in the PV distribution and its effects on subsurface temperature variations have not been investigated previously.

Motivated by these observational and GCM studies, we investigate the steady response of the thermocline to an anomalous Ekman pumping, focusing on the effects of MLD distribution that features a sharp gradient in the northwestern subtropical gyre. We use a ventilated thermocline model that allows easy modification of MLD distribution and easy interpretation of the results. Following Inui *et al*. (1999), we focus on a case where the changes of Ekman pumping are limited to the northern half of the subtropical gyre, corresponding to an intensification of the westerlies. We show that the Inui *et al*. results can be reproduced to a large extent without any anomalous changes in the MLD distribution.

Huang and Pedlosky (1999) studied a similar problem of oceanic response to anomalous Ekman pumping using the LPS model without a surface mixed layer. Most recently, Huang (2000) used a continuously stratified model that includes an MLD distribution, but its gradient is quite weak compared to that seen in the real ocean and in ocean GCMs. In our model, there is a so-called MLD front where MLD varies rapidly from deep in the northwestern subtropical gyre to shallow elsewhere. This sharp MLD gradient in the mean state strongly affects the PV distribution and is shown to have a large impact on the response of the ocean to anomalous changes in Ekman pumping. The present paper considers only a steady response of oceanic thermocline to an anomalous Ekman pumping. Recent works on the time-dependent adjustment of the thermocline show that Ekman pumping anomaly can yield the higher baroclinic modes in the south of the forcing region in transient stage, even when the surface density condition is zonally uniform (Nagakura, 1999; Dewar and Huang, 2001; Kubokawa and Nagakura, 2002), so that some caution may be needed when applying the present result to observations.

Section 2 gives a brief description of the ventilated thermocline model used here. Section 3 presents and contrasts the results from solutions with and without the MLD front. Section 4 is reserved for a summary and remarks. In addition, Appendix gives the solutions in a new coordinate system using the Sverdrup function as the zonal coordinate, which offers better insights into the anomaly generation mechanism than that presented in Section 3.

2. Ventilated Thermocline Model

The ventilated thermocline model is formulated in terms of the isopycnal coordinates (x, y, ρ), where x, y and ρ are the eastward, northward and density coordinates, respectively. Although we treat the problem in the β plane, there is no essential difference from that in spherical coordinates. The basic equations are the geostrophic and hydrostatic balances, the conservation of the potential vorticity along the geostrophic streamline, and a zonally integrated Sverdrup equation:

$$-fv = -\frac{1}{\rho_0}\frac{\partial B}{\partial x}, \quad fu = -\frac{1}{\rho_0}\frac{\partial B}{\partial y}, \tag{1}$$

$$\frac{\partial B}{\partial \rho} = gz, \tag{2}$$

$$\frac{\partial z}{\partial \rho} = -fq(B,\rho), \tag{3}$$

$$\int_{\rho_s}^{\rho_b} z^2 d\rho - \int_{\rho_s^e}^{\rho_b} z^{e2} d\rho = 2\phi, \tag{4}$$

where f is the Coriolis parameter, B is the Bernoulli function which is the geostrophic stream function on isopycnal surfaces, z is the depth of the isopycnal of density ρ (z is zero at the sea surface and decreases downward), q is the potential thickness (reciprocal of the potential vorticity), the subscripts s and b and superscript e denote the values at the sea surface, a deep layer below which the fluid is at rest and the eastern boundary, respectively, and ϕ is the Sverdrup function defined by

$$\phi = \frac{\rho_0 f^2}{\beta g} \int_{x^e}^{x} w_e dx. \quad (5)$$

Here, w_e is the Ekman pumping velocity at the bottom of a thin surface Ekman layer. The isopycnal depth at the eastern boundary below the mixed layer, z^e, is assumed to be a prescribed function of only ρ, as in Huang and Russell (1994). The upper boundary conditions for Eqs. (2) and (3) is

$$z = z_m \quad \text{at} \quad \rho = \rho_s \quad (6)$$

where z_m is the prescribed depth of the base of the mixed layer, and the lower boundary condition is

$$z = z^e(\rho_b), \quad B = B^e(\rho_b) \quad \text{at} \quad \rho = \rho_b. \quad (7)$$

The ventilated thermocline structure is obtained by solving Eqs. (2)–(4) from the north to south. The above model equations are the same as those derived by Huang and Russell (1994), and we use the same method to solve these equations as in Kubokawa (1999). Here we outline how $q(B, \rho)$ is determined in the model, because it is crucial in understanding subsequent results.

The potential thickness of the ventilated fluid, $q(B, \rho_s)$, can be determined by solving Eqs. (2) and (3) with respect to Eqs. (6) and (7), since $q(B, \rho)$ is already known for $\rho > \rho_s$. This implies that if the mixed layer shoals in the direction of geostrophic flow at the base of the mixed layer, the subducted fluid will be thick compared with the case with uniform z_m (see Williams, 1989). This effect of the mixed layer depth distribution on the potential vorticity is very important in the present study. For deep unventilated layers that do not outcrop in the subtropical gyre, $q(B, \rho)$ in a moving layer is assumed to be homogenized at the value at the northern edge of the subtropical gyre (Young and Rhines, 1982). For shallow isopycnals outcropping in the subtropical gyre, the potential vorticity along the streamline emanating from the western boundary is assumed to be homogenized at the value at $(x^w, y_s(x^w, \rho))$, where x^w is the location of the western boundary and $y_s(x^w, \rho)$ is the outcrop latitude of the isopycnal labeled by ρ. The latter homogenized region in the shallow isopycnals is labeled hereafter as the pool region, following Luyten *et al*. (1983).

The present study makes further simplifications as in Kubokawa (1999):

1. The basin is rectangular and neither cross gyre ventilation nor eastern boundary ventilation are included.
2. $dz^e/d\rho$ is constant for $\rho > \rho_0$, where ρ_0 is the density of the isopycnal outcropping at the sea surface at the northern boundary of the subtropical gyre. This condition enables us to obtain the analytic solution for the deep unventilated layer, so that the model is required to solve equations numerically only for $\rho \le \rho_0$.
3. The density structure in the ventilated layer where $\rho \le \rho_0$ is approximated by a small number of isopycnal surfaces (seven layers in this article).
4. The meridional gradient of surface density is assumed to be constant, and the surface density is longitudinally uniform.

The variables are nondimensionalized as follows:

$$f^* = \frac{f}{f_0}, \quad \beta^* = \frac{\beta}{f_0 L_y}, \quad q^* = \frac{f_0 \alpha q}{H}, \quad x^* = \frac{x}{L_x}, \quad y^* = \frac{y}{L_y},$$
$$z^* = \frac{z}{H}, \quad \phi^* = \frac{\phi}{\alpha H^2}, \quad B_j^* = \frac{B_j}{\alpha g H}, \quad w_e^* = \frac{\rho_0 f_0^2 L_x}{\alpha \beta g H^2} w_e, \quad (8)$$

where f_0 is the Coriolis parameter at the northern edge of the subtropical gyre, L_y is the north-south extent of the subtropical gyre, L_x is the ocean width, H is the maximum thickness of the mixed layer, and α/L_y gives the meridional gradient of the surface density. The asterisks denoting the nondimensional variables are dropped in the following discussion. The nondimensional β and $dz^e/d\rho$ are set to be 0.7 and 3, respectively, as in Kubokawa (1999).

3. Method and Results

The present brief article discusses the difference between the steady solutions with and without w_e anomaly. We compare two cases: CASE I in which ρ_s and z_m are zonally uniform and CASE II in which z_m is allowed to vary in the longitudinal direction. In each case, we keep the distributions of ρ_s and z_m the same, but vary the strength and lateral distribution of w_e.

The Ekman pumping velocity, w_e, is assumed for simplicity to have the form $w_e = \beta f^{-2}(w_0 + w_1)$, where $w_0(y) = W_0 \sin \pi y$ represents the basic state and $w_1(y)$ is an anomaly which is zero for the standard w_e case and is

$$w_1(y) = \begin{cases} W_1 \sin 2\pi y & \text{for } y \ge -0.5 \\ 0 & \text{otherwise,} \end{cases} \quad (9)$$

for the enhanced w_e case. In the following computations we set $W_0 = 0.5$ and $W_1 = 0.3W_0$. This value of W_0 gives a basin width of about 6000 km, if we assume that $H = 300$ m and the other parameters are the same as those used in Kubokawa (1999). We increase the Ekman pumping only in the northern half of the gyre, which corresponds to an intensified westerly wind. We additionally consider a case in which the Ekman pumping is enhanced over the whole subtropical gyre (CASE II′ in Subsection 3.3).

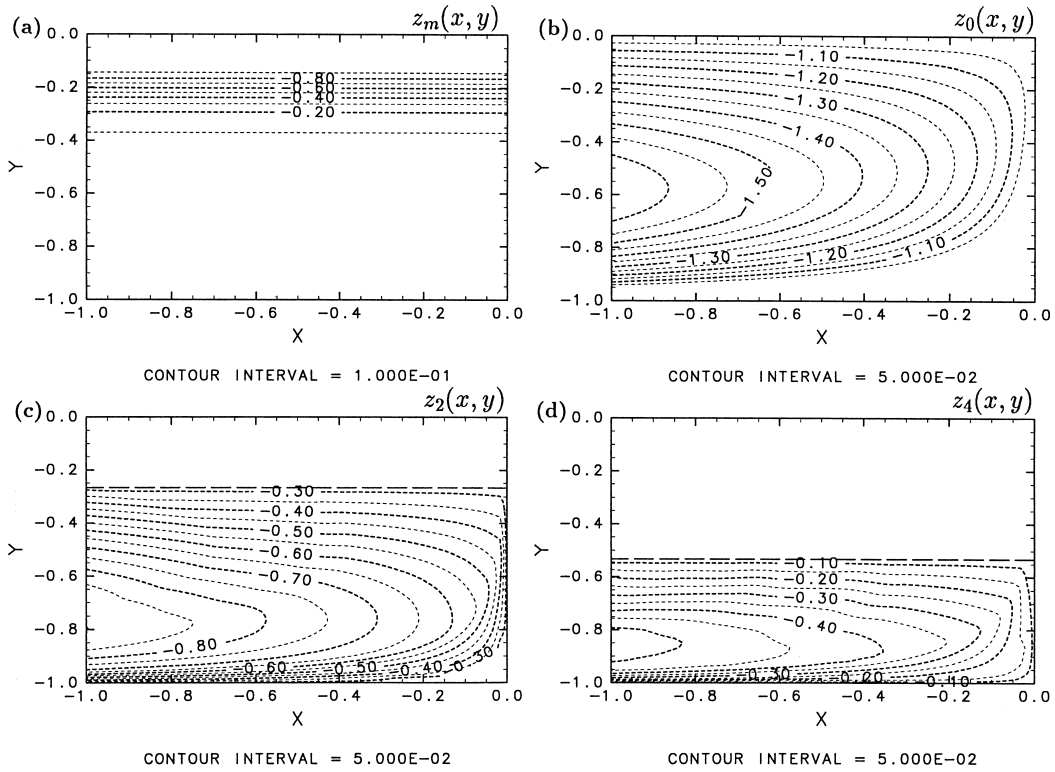

Fig. 1. Specified mixed layer depth and the depth distributions of the isopycnal surfaces for CASE I with standard w_e forcing: (a) $z_m(x, y)$, (b) $z_0(x, y)$, (c) $z_2(x, y)$ and (d) $z_4(x, y)$. The horizontal dashed line in the lower two panels denotes the outcrop latitude, and the z_0 surface outcrops at $y = 0$. The contour interval is given below each panel.

3.1 CASE I: Zonally uniform mixed layer depth

Figure 1(a) shows the mixed layer depth (MLD) distribution. The surface density is assumed to be zonally uniform and is a linear function of y. Panels (b)–(c) show the depth distributions on isopycnals, z_0, z_2 and z_4 in the standard w_e case, in which w_1 is set to zero. The isopycnal surface labeled number "0" outcrops at the northern boundary of the subtropical gyre and other isopycnals are numbered in the order of decreasing density. Figure 2 depicts the depth difference between the enhanced w_e and the standard w_e cases on the deepest four isopycnals. When w_e is enhanced for $y > -1/2$, the deep isopycnals, z_0 and z_1, deepen there, although the difference is small (note that the contour interval is 0.01 or 3 m if we assume H = 300 m). This warming arises from the intensified Sverdrup current confined in the latitude band where w_e is enhanced. In this case, the potential thickness functional relation, $q(B, \rho)$, does not change before and after the increased Ekman pumping (Appendix). On the other hand, anomalies of shallower isopycnal depths can be seen south of where anomalous w_e is imposed. This is because of the changes in the boundary of the pool region in each layer and its potential vorticity. The pool region extends slightly eastward and its potential vorticity decreases slightly. The change in pool region also affects the potential vorticity of fluid ventilated above it. Therefore, in summary, when the mixed layer depth is zonally uniform, the subsurface density anomalies are produced by the direct effect of the Sverdrup flow change and the change in the pool region, but these anomalies are small.

3.2 CASE II: Zonally varying mixed layer depth

When the mixed layer depth (MLD) is not zonally uniform, the solution changes drastically. In the present article we adopt an MLD distribution similar to that in the ocean GCM experiment by Inui *et al*. (1999). In their experiment the mixed layer deepens abruptly in the northern half of the subtropical gyre and this transition zone between the deep and shallow mixed layer depths inclines northeastward. We refer to this transition zone as an MLD front hereafter. Figure 3 shows the depth distributions of the mixed layer and the isopycnals, z_0, z_2 and z_4 under the standard w_e forcing. In this case the isopycnal, z_2, does not deepen monotonically westward but instead has a shallow region extending southwestward. This distortion of the density structure is caused by a strong inhomogeneity of potential vorticity below the z_2 surface. As mentioned in Section 2, the potential vorticity (PV) of venti-

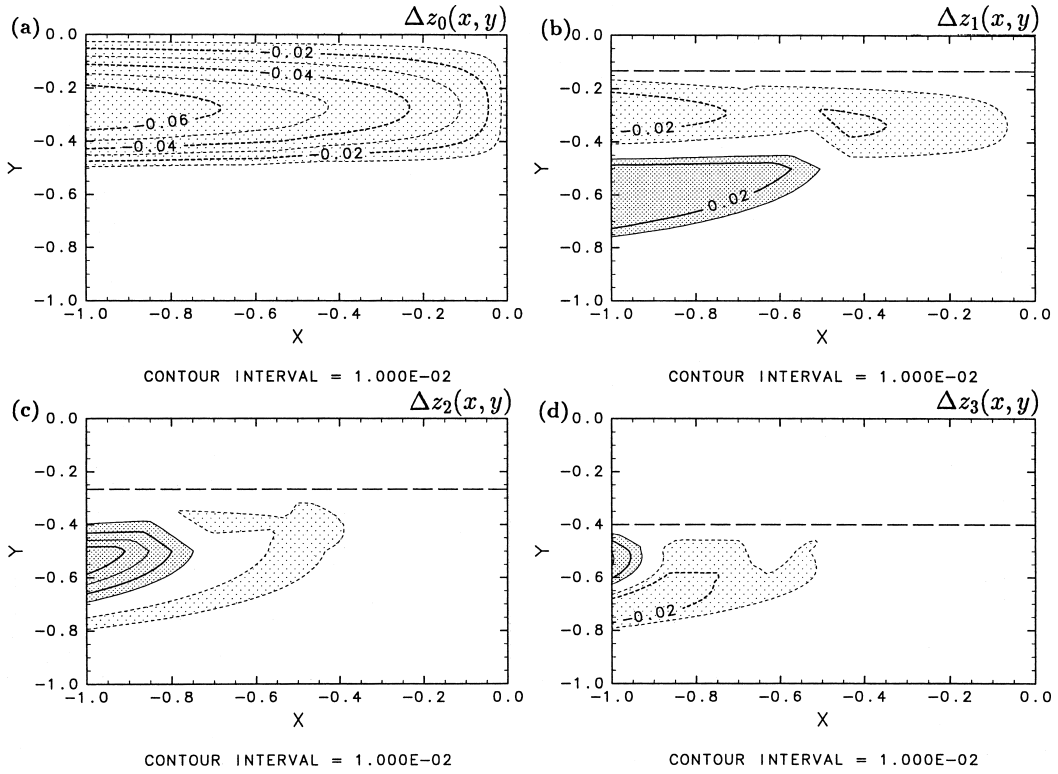

Fig. 2. Difference of the isopycnal depth of the enhanced w_e case from the standard case: (a) $\Delta z_0(x, y)$, (b) $\Delta z_1(x, y)$, (c) $\Delta z_2(x, y)$ and (d) $\Delta z_3(x, y)$. Contour interval is 0.01, and the light and heavy shades denote the regions of $\Delta z_j < -0.01$ and $\Delta z_j > 0.01$, respectively. The zero contours are omitted. The horizontal dashed line in each panel denotes the outcrop latitude.

lated fluid is strongly affected by the gradient of MLD along the current, so that the minimum PV between two isopycnals is formed around the longitude where the MLD front exists between these two outcrops. Since the surface current is southeastward in the northern half of the subtropical gyre, the low PV source for each layer occurs at the eastern side of the intersection of the outcrop of shallower isopycnal surface and the MLD front. As it moves south, this low PV fluid pushes up its upper interface and causes it to shallow (see Fig. 5(a) for a zonal section). Kubokawa (1999) suggested that this low PV fluid corresponds to the subtropical mode water, and generates a subtropical countercurrent along its southern edge.

Figure 4 depicts the isopycnal depth anomalies due to enhanced w_e for the deepest four isopycnals. Note that the contour intervals here are five times larger than those in Fig. 2. The effect of the MLD distribution on the anomalies on the surface z_0 is insignificant, i.e., the surface z_0 deepens for $y > -1/2$ but is almost unchanged for $y \leq -1/2$, similar to CASE I. The shallower isopycnals, however, shoal significantly, leading to a cooling that extends southwestward. The line of the maximum depth anomaly tends to shift westward from a denser isopycnal to a lighter one. This strong subsurface cooling south of the anomalous Ekman-pumping forcing is very similar to that in Inui *et al.*'s (1999) ocean GCM, but without any anomalous change in MLD.

Figure 5(a) shows the zonal section of the density (zonal distributions of isopycnal depths) at the central latitude of the subtropical gyre, $y = -1/2$. Both before and after Ekman pumping is increased, the layer thickness has a local maximum indicative of low PV fluid that is formed to the north near the intersection of the MLD front and the outcrop line. Since this intersection moves eastward as the surface density increases, the low PV regions move successively toward the east from light to dense isopycnals in this zonal section.

In response to enhanced Ekman pumping to the north, the maximum depth anomaly of an isopycnal (the difference between the solid and dashed lines) at $y = -0.5$ occurs near the western edge of the low PV water in the layer immediately below (i.e., at $x \simeq -0.3$ for z_1, -0.55 for z_2 and -0.85 for z_3). This association of anomalous subsurface cooling with the PV minimum suggests that it is caused by an anomalous westward shift of low PV fluids. Figure 5(b) shows the PV distributions in the layer between z_1 and z_2 for both the standard and enhanced w_e

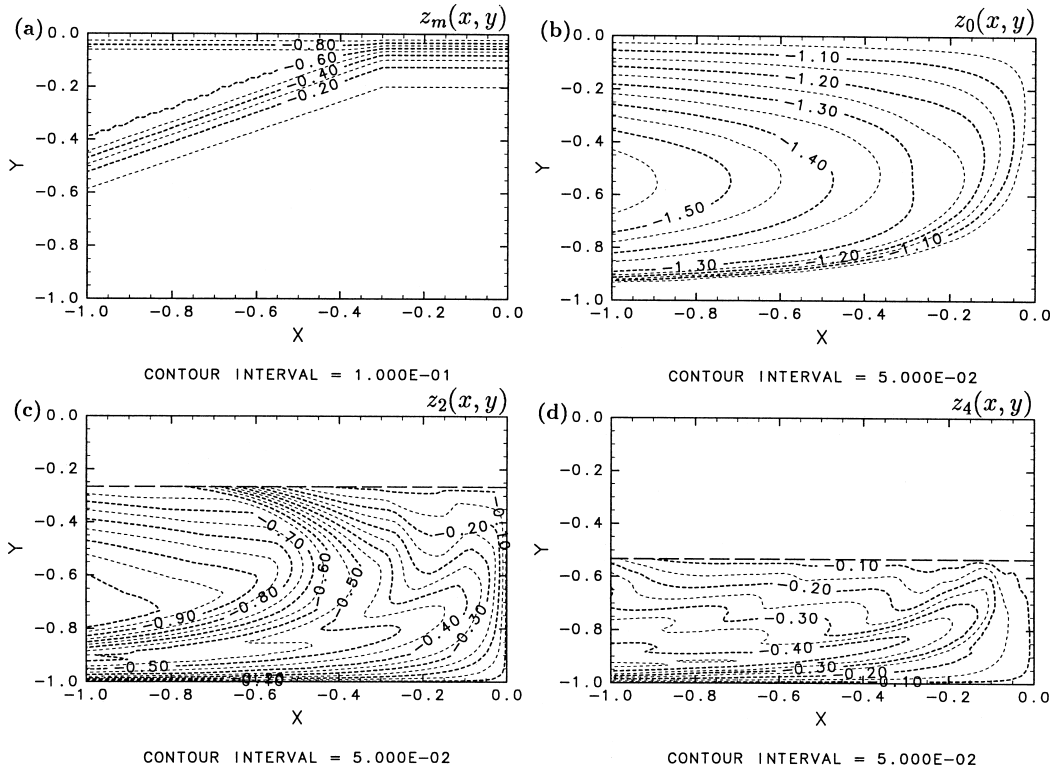

Fig. 3. Same as Fig. 1 but for CASE II in which the mixed layer depth contours slant northeastward.

cases, along with the z_2 anomaly. The low PV water forms at the same longitudes at the outcrop latitude because neither surface density nor MLD change between the two cases. As the low PV water moves southward, its path shift anomalously westward in response to the increased Ekman pumping. Since the PV is conserved along the streamlines on isopycnal surfaces, this change in PV distribution is due to a westward shift of particle trajectories. Significant depth anomalies in Fig. 5(b) are bounded by the boundaries of the low PV water in the enhanced w_e case, reaffirming that the subsurface cooling results from anomalous change in the path of the PV minimum.

3.3 A qualitative explanation for CASE II

Why does the low PV fluid shift its path westward in the southern subtropics in response to an anomalous Ekman forcing confined to the north? To address this question, let us first consider the trajectory of a particle advected by the Sverdrup flow. If w_e is only a function of y as is assumed here, such a trajectory satisfies

$$\frac{dx}{dy} = -\frac{\partial\phi/\partial y}{\partial\phi/\partial x} = -\frac{\beta\left(x - x^e\right)}{f^2 w_e}\frac{\partial}{\partial y}\left(\frac{f^2}{\beta}w_e\right). \qquad (10)$$

Integrating Eq. (10), we get the trajectory of a particle starting from (x_0, y_0) as

$$x(y) = x^e + \left(x_0 - x^e\right)\frac{f^2(y_0)w_e(y_0)}{f^2(y)w_e(y)}. \qquad (11)$$

Therefore, the longitudinal change in trajectory due to the enhanced w_e becomes

$$\Delta x(y) = \left(x_0 - x^e\right)\frac{w_0(y)w_1(y_0) - w_0(y_0)w_1(y)}{\left(w_0(y) + w_1(y)\right)w_0(y)}. \qquad (12)$$

Since $w_1(-1/2) = 0$ and $x_0 - x^e < 0$, $\Delta x(-1/2) = (x_0 - x^e)w_1(y_0)/w_0(-1/2)$ is always negative irrespective of the starting point, (x_0, y_0), in CASE II. Physically, this westward shift of fluid trajectories is caused by the anomalous Sverdrup flow that is westward south of the w_1 maximum. Only for a fluid particle that starts at the northern boundary ($y_0 = 0$), does the advection by the anomalous eastward Sverdrup flow north of the w_1 maximum exactly cancel the westward advection to the south, and $\Delta x(-1/2) = 0$. In the southern subtropical gyre where $w_1 = 0$, the Sverdrup flow remains the same before and

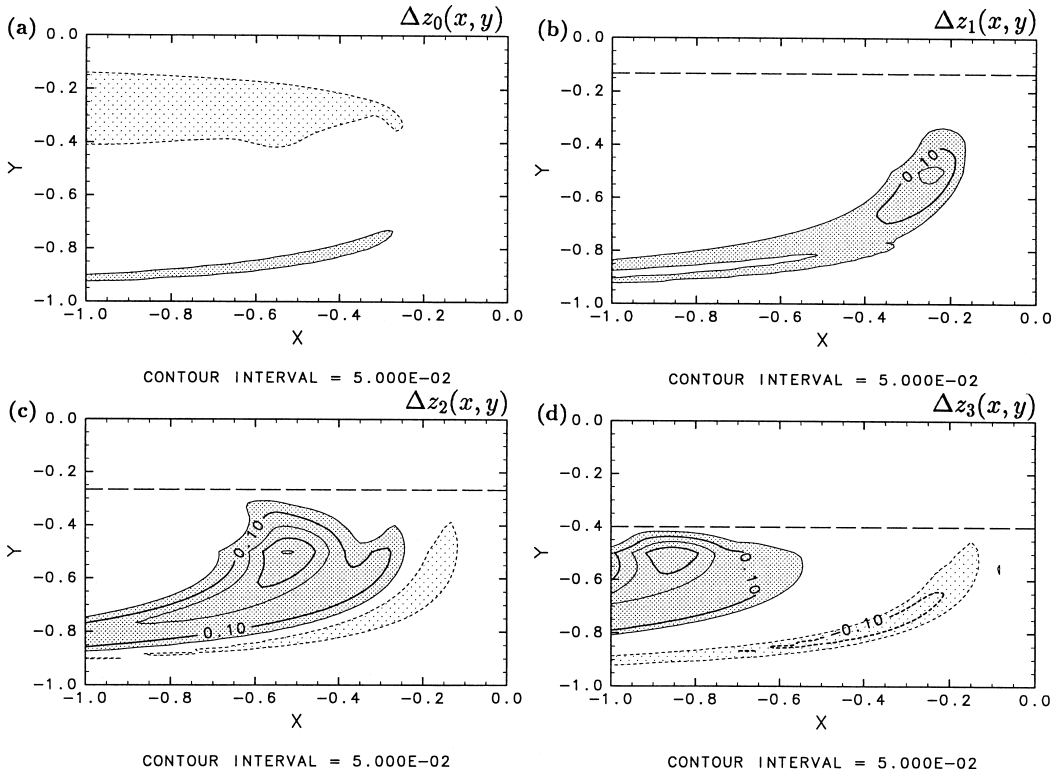

Fig. 4. Same as Fig. 2, but for CASE II. Contour interval is 0.05, and the light and heavy shades denote the regions of $\Delta z_j < -0.05$ and $\Delta z_j > 0.05$, respectively.

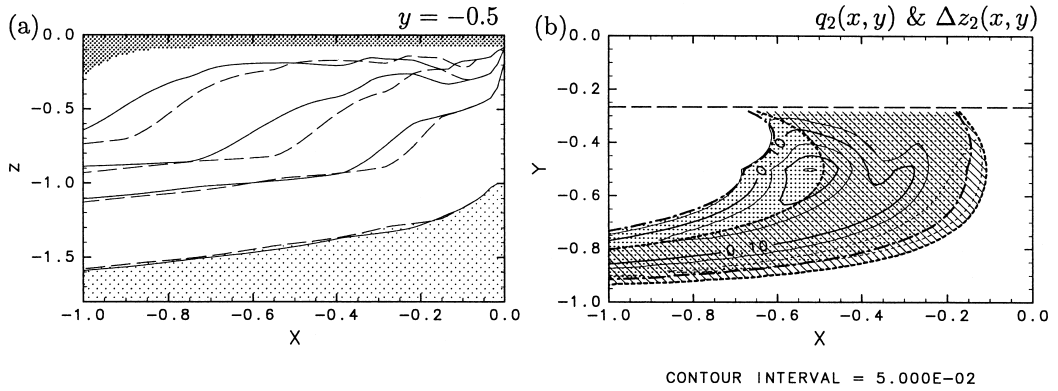

Fig. 5. (a) Zonal distributions of the isopycnal depths at $y = -0.5$ for CASE II, and (b) the distributions of low potential vorticity fluids in the layer between z_1 and z_2 superimposed on the z_2 anomaly. In panel (a), dashed lines denote the isopycnals in the standard case, while the solid lines denote those in the enhanced w_e case. The heavy and light shades denote the mixed layer and the unventilated layer, respectively. In panel (b), the shade by slashes (dots) denotes the low PV region where $(z_2 - z_1)/f \geq 0.35$ for the standard (enhanced) w_e case. The thick dotted and dash-dotted lines denote the contours of $(z_2 - z_1)/f = 0.35$ for these two cases, respectively.

after the anomalous Ekman pumping is applied to the north. But Δx is still non-zero because the particle leaves $y = -1/2$ at different longitudes ($\Delta x(-1/2) < 0$).

This Sverdrup argument is consistent with the anomalous shift of PV minima on isopycnal surfaces in CASE II. Its success as a qualitative explanation for CASE II is rooted in the fact that the gyre-scale adjustment in response to a wind change is captured to a large extent by

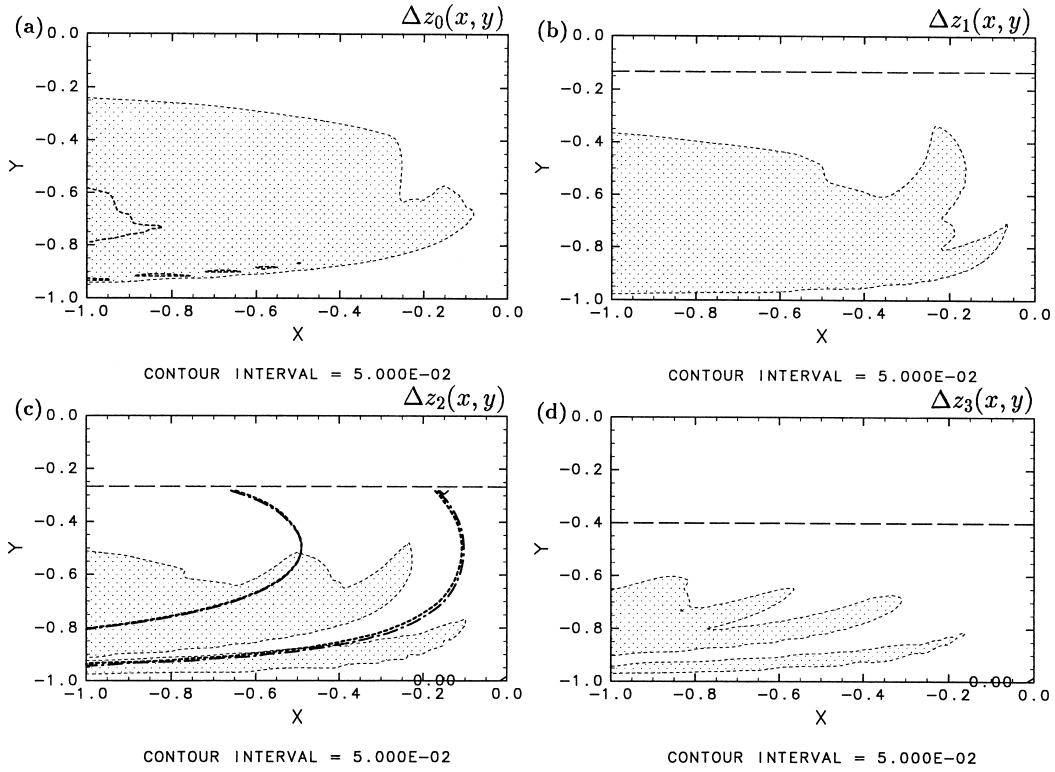

Fig. 6. Same as Fig. 4, but for w_e is enhanced in the whole subtropical gyre: $w_1 = W_1 \sin \pi y$. The shade denotes the regions of $\Delta z_j < -0.05$. The thick dotted lines and dash-dotted lines denote the contours of $(z_2 - z_1)/f = 0.35$ for the standard and enhanced w_e cases, respectively.

the Sverdrup theory. Quantitatively, however, the above argument is still quite crude as anomalous flows on different isopycnals change both the speed and direction due to the beta-spiral effect. Appendix presents a more precise explanation based on so-called Sverdrup coordinates.

The above argument predicts that if $w_1(y)$ has the same functional form as $w_0(y)$, the depth anomalies will be small because $\Delta x(y) = 0$. To test this prediction, we make an additional computation (CASE II′) by letting $w_1(y) = W_1 \sin \pi y = (W_1/W_0) w_0(y)$. Indeed, the changes in both the isopycnal PV and depth distributions are all much reduced in comparison to CASE II where the Ekman pumping anomaly is confined to the northern half of the subtropical gyre (Fig. 6 vs. Fig. 4). This success of the prediction based on Eq. (12) suggests that the Sverdrup argument captures some essence of the response mechanism. In contrast to CASE II, a weak warming takes place over the whole subtropical gyre and on all the isopycnal surfaces as a result of the first baroclinic mode response to the w_e anomaly.

3.4 Dependence on the width of MLD front

As shown in the preceding subsections, the significant anomalies of the isopycnal depths in CASE II are caused by the westward shift of the low PV fluid subducted around the intersection of the MLD front and the outcrop line. In this subsection we examine the sensitivity of the result to the width of the MLD front. Figure 7 shows the dependence of the maximum depth anomaly of each isopycnal surface on the meridional scale of the MLD front. The case that the width is 0.1 corresponds to CASE II shown in Fig. 4. The anomaly pattern itself is not sensitive to the width of the MLD front (not shown). The magnitude of the anomaly, however, strongly depends on and is nearly proportional to the inverse of the meridional width. This can easily be understood as follows. In this system, the isopycnal depth anomaly is caused by the westward shift of the fluid trajectory which is dominated by the change in the Sverdrup flow, so that the magnitude of the anomaly must be proportional to the longitudinal gradient of the potential thickness (see Fig. 5(a)). The longitudinal gradient of the potential thickness is mainly caused by the gradient of the MLD along the outcrop line. Since the longitudinal gradient of the MLD is proportional to the meridional gradient of the MLD, the magnitude of the isopycnal depth anomaly is nearly proportional to the inverse of the meridional width of the MLD front, as seen in Fig. 7.

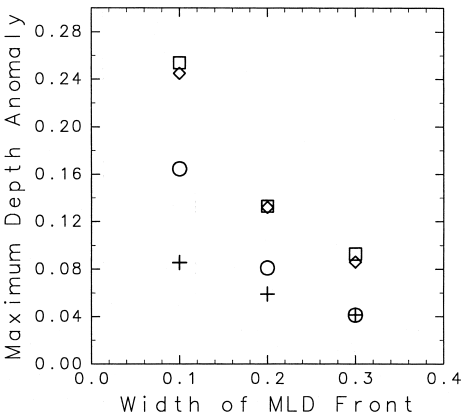

Fig. 7. Dependence of the maximum depth anomaly of each isopycnal surface on the width of the MLD front: Δz_1 (+), Δz_2 (○), Δz_3 (□), Δz_4 (◇), CASE II corresponds to the width = 0.1. The functional form of the MLD distribution used in this paper is the same as in Kubokawa (1999), and the horizontal axis in this figure is $\gamma_0^{-1/2}$ in (4.4) in Kubokawa (1999).

4. Summary and Remarks

In the present article we have investigated the steady response of the ocean thermocline to an increase in Ekman pumping that is confined to the northern half of the subtropical gyre. The thermocline slightly deepens in the latitude band where the Ekman pumping is increased, much as one can expect from the response of the first baroclinic mode Rossby wave. In addition to this local effect, a remote response is also found in the southern subtropical gyre where the anomalous forcing vanishes and no first mode Rossby wave is excited. In particular, when there is a sharp MLD front in the model climatology, a pronounced subsurface cooling occurs in the ventilated thermocline along the characteristics in the forcing-free southern subtropics. This cooling is attributed to the changes in the path of the low potential vorticity fluid formed near the intersection of the outcrop line and the MLD front. We suggest that the changes in the PV distribution are in turn mainly due to those in the advection by the Sverdrup flow. As the low potential vorticity fluids move westward, they push up the isopycnals above them and cause cooling. This advective mechanism can operate without any anomalous changes in MLD that is at the heart of the mechanism proposed by Inui *et al*. (1999) for subsurface cooling. In their mechanism, MLD changes shift the formation region of the low PV fluid, leading to changes in their subsequent paths. In reality, these two mechanisms are likely to operate cooperatively and give rise the strong cooling reported in their GCM experiment.

Very recently, Xie *et al*. (2000) forced an ocean GCM of the North Pacific with the observed wind stress for the past four decades and reported that the changes in the path of low potential vorticity mode waters are a major cause of the subsurface density variability in the model subtropics. They speculated that both Inui *et al*.'s and the advective mechanisms may be responsible for the anomalous zonal excursion of mode waters in their GCM simulation. Our calculation has demonstrated that the latter can indeed be operational without MLD anomalies.

The present study considered only the effect of zonal MLD variations on the thermocline response to a change in Ekman pumping velocity. The response has higher baroclinic mode structures in the vertical (see Fig. 5(a)) despite the absence of anomalous density forcing. Such higher baroclinic mode response to anomalous w_e is also possible if the surface density is not zonally uniform, as is discussed by Huang and Pedlosky (1999). Surface density and MLD distributions are key to determining the potential vorticity of a ventilated fluid, and an anomalous Ekman pumping changes the advection of potential vorticity, which in turn causes subsurface density anomalies. Generally, it can be shown that an anomalous w_e has a similar effect to imposing a surface density anomaly if either surface density or mixed layer depth varies in the zonal direction (Appendix).

Acknowledgements

The authors thank the reviewers for their valuable comments. This work was financially supported by the Japanese Ministry of Education, Science and Culture, and the Japan Society for the Promotion of Science. This is IPRC contribution No. 145 and SOEST contribution No. 5917. The GFD-DENNOU Library was used for drawing the figures.

Appendix: Solutions in the Sverdrup Coordinates

A coordinate transformation that replaces x with a single-valued function $\phi(x, y)$ can cast the solutions of the thermocline equations, $B(x, y, \rho)$ and $z(x, y, \rho)$, into forms of $B(\phi, y, \rho)$ and $z(\phi, y, \rho)$. Here we choose ϕ to be the Sverdrup function defined by Eq. (5). This transformation eliminates the explicit dependence on w_e because Eqs. (2)–(4) explicitly depend neither on x nor w_e but on ϕ, and the boundary conditions at the sea surface Eqs. (6)–(7) and at the eastern boundary can all be written in terms of (ϕ, y, ρ). We refer to (ϕ, y, ρ) as the Sverdrup coordinate system (Kubokawa, 1995). This coordinate system is not entirely new; analytic solutions of the LPS model (Luyten *et al*., 1983) are often written as functions of the Sverdrup function and f, and their dependence on x and w_e appears only through the Sverdrup function $\phi(x, y)$. This transformation involves only the horizontal axes and does not make any a priori assumption on the vertical structure of flow velocity. In fact, the baroclinic flow structure will come out as part of the solution. As

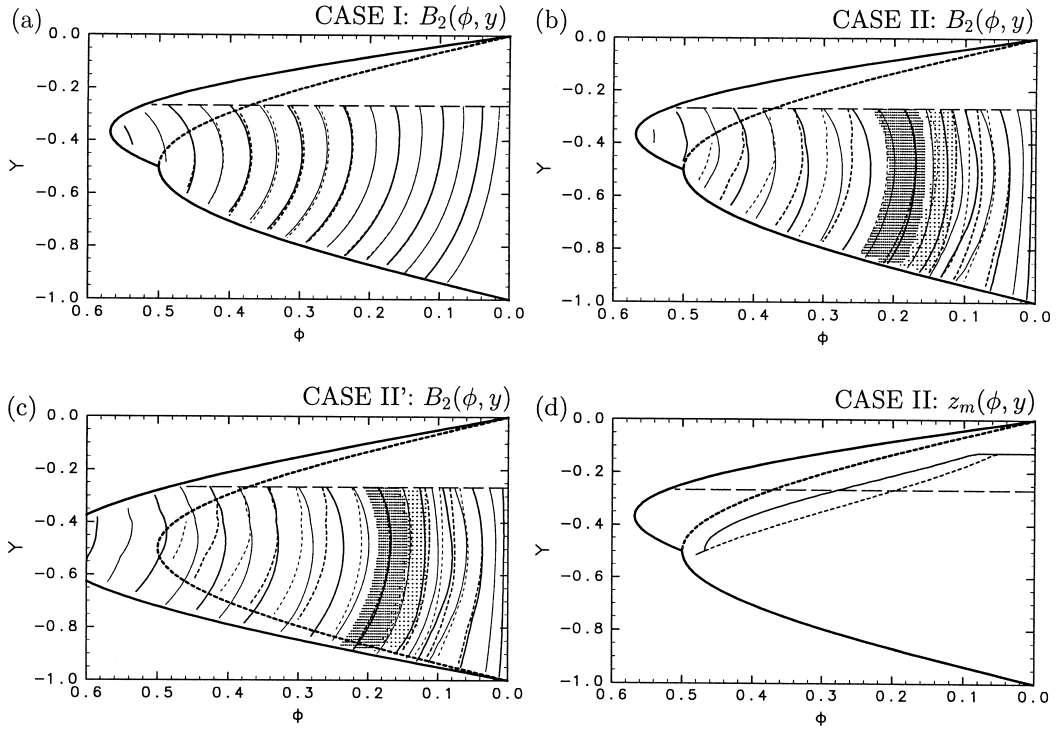

Fig. A1. Distribution of the Bernoulli function in the layer between z_1 and z_2 in the Sverdrup coordinates for (a) CASE I, (b) CASE II and (c) CASE II′. Panel (d) shows the contour where the mixed layer depth is 0.2. In all the panels, those for both the standard w_e case (dotted lines) and the enhanced w_e case (solid lines) are plotted. The thick dotted and solid curves denote the location of the western boundary for standard and enhanced w_e cases, respectively, and the eastern boundary exists at ϕ = 0. The shaded regions in Panels (b) and (c) denote the minimum potential vorticity regions where potential thickness, $(z_2 - z_1)/f$, is larger then 0.775 for the standard w_e case (light shade) and 0.795 for the enhanced w_e case (heavy shade). The contour interval for the Bernoulli function is 0.02 for all the panels. The horizontal dashed line denotes the outcrop latitude of z_2 interface.

will become clear, this Sverdrup coordinate system has certain advantages in understanding solution behavior.

The transformation from Sverdrup coordinates to (x, y) coordinates, when w_e is only a function of y as is in this study, can be simply done by

$$x = x^e + \frac{x^w - x^e}{\phi^w(y)}\phi, \tag{A.1}$$

where ϕ^w is the ϕ coordinate of the western boundary:

$$\phi^w(y) = \frac{f^2}{\beta}\left(x^e - x^w\right)w_e(y). \tag{A.2}$$

Therefore, an enhancement of w_e pushes the western boundary (ϕ^w) to the west in Sverdrup coordinates, and the zonal distribution of mixed layer depth is also stretched westward, because $z_m(\phi, y) = z_m(f^2\beta^{-1}(x^e - x)w_e(y), y)$ (Fig. A1). That is, a change in w_e affects the solutions in Sverdrup coordinates through the changes in ϕ^w and $z_m(\phi, y)$ in the present model.

In CASE I, surface boundary conditions are zonally uniform and thus remain the same in the standard and the enhanced w_e cases in Sverdrup coordinates. The only difference is in the stretched western boundary, which causes small changes in the Bernoulli function in the western region (Fig. A1(a)). In the eastern region, the solutions are identical to each other in the (ϕ, y) plot because the functional relation between the potential thickness and the Bernoulli function, $q(B, \rho)$, is the same. Transformed into real space, the solution becomes dependent on w_e, because $B(\phi, y, \rho) = B(f^2\beta^{-1}(x^e - x)w_e(y), y, \rho)$. An increased w_e is equivalent to displaying B in a compressed x-coordinate at a compression rate of w_e. Because this coordinate compression rate is independent of density, the resultant anomalies have a first baroclinic mode structure in real space.

In CASE II, the mixed layer depth front moves westward in response to the enhanced w_e, and so does the source of the low potential vorticity in the (ϕ, y, ρ) space,

resulting in large differences in $q(B, \rho)$. Because the streamlines remain nearly the same before and after the w_e increase (Fig. A1(b)), the trajectories of PV minima (the shaded regions in Fig. A1(b)) are almost parallel, too. If we transfer these distributions into (x, y) coordinates, the trajectory differences are small in the northern half where the increased w_e compresses the real space, while the PV differences remain large in the south. These PV anomalies lead to large subsurface density anomalies in (x, y) coordinates because of the great slope of isopycnals west of the PV minima. The qualitative argument presented in Section 3 is based on this consideration. Since this mechanism most strongly affects those mode waters that form at latitudes of large anomalous w_e, the subsurface anomalies are localized within a certain density range and thus have higher baroclinic structures.

In CASE II′, the low potential vorticity source also shifts westward in Sverdrup coordinates in the enhanced w_e case (Fig. A1(c)). Since the w_e is enhanced at all the latitudes, however, the difference in the trajectories is reduced everywhere when the solution is transferred into (x, y) coordinates because of space compression. Therefore, in spite of the difference in $q(B, \rho)$, the depth anomalies are small in this case in real space.

The above Sverdrup-coordinate-based thinking implies that the higher baroclinic mode response needs a change in the functional relation between the potential thickness and the Bernoulli function, $q(B, \rho)$; without $q(B, \rho)$ change, only the first baroclinic mode response is possible (the eastern region in CASE I). When the surface boundary conditions for density structure vary in the zonal direction, a w_e anomaly can yield a significant change in $q(B, \rho)$, because the wind anomaly modifies them in Sverdrup coordinates (CASE II). This modification of the surface density boundary conditions in Sverdrup coordinates induced by anomalous w_e has the same effect as a surface density forcing without w_e anomaly on $q(\mathrm{B}, \rho)$. Therefore, the response to an Ekman pumping anomaly in such a situation can be similar to that of a surface density forcing anomaly, although its appearance in real space depends on an anomalous wind pattern (CASE II vs. CASE II′). It should also be noted that the present argument is applicable even when the w_e anomaly is a function of x as well as y, because the solutions in Sverdrup coordinates do not depend on w_e itself.

References

Deser, C., M. A. Alexander and M. S. Timlin (1996): Upper-ocean thermal variations in the North Pacific during 1970–1991. *J. Climate*, **9**, 1840–1855.

Dewar, W. K. and R. X. Huang (2001): Adjustment of the ventilated thermocline. *J. Phys. Oceanogr.*, **31**, 1676–1697.

Huang, R. X. (2000): Climate variability inferred from a continuously stratified model of the ideal-fluid thermocline. *J. Phys. Oceanogr.*, **30**, 1389–1406.

Huang, R. X. and J. Pedlosky (1999): Climate variability inferred from a layered model of the ventilated thermocline. *J. Phys. Oceanogr.*, **29**, 779–790.

Huang, R. X. and S. Russell (1994): Ventilation of the Subtropical North Pacific. *J. Phys. Oceanogr.*, **24**, 2589–2605.

Inui, T., K. Takeuchi and K. Hanawa (1999): A numerical investigation of the subduction process in response to an abrupt intensification of westerlies. *J. Phys. Oceanogr.*, **29**, 1993–2015.

Kubokawa, A. (1995): Stationary Rossby waves and shocks on the Sverdrup coordinate. *J. Oceanogr.*, **51**, 207–224.

Kubokawa, A. (1999): Ventilated thermocline strongly affected by a deep mixed layer: A theory for subtropical countercurrent. *J. Phys. Oceanogr.*, **29**, 1314–1333.

Kubokawa, A. and T. Inui (1999): Subtropical countercurrent in an idealized ocean GCM. *J. Phys. Oceanogr.*, **29**, 1303–1313.

Kubokawa, A. and M. Nagakura (2002): Linear planetary wave dynamics in a 2.5-layer ventilated thermocline model. *J. Mar. Res.* (in press).

Liu, Z. (1999): Forced planetary wave response in a thermocline gyre. *J. Phys. Oceanogr.*, **29**, 1036–1055.

Luyten, J. R., J. Pedlosky and H. Stommel (1983): The ventilated thermocline. *J. Phys. Oceanogr.*, **13**, 292–309.

Nagakura, M. (1999): Waves in a 2.5-layer ventilated thermocline model and oceanic response to atmospheric forcing. Master Thesis, Hokkaido University, 131 pp. (in Japanese).

Nonaka, M., S.-P. Xie and K. Takeuchi (2000): Equatorward spreading of a passive tracer with application to North Pacific interdecadal temperature variations. *J. Oceanogr.*, **56**, 173–183.

Schneider, N., S. Venzke, A. J. Miller, D. W. Pierce, T. O. Barnett, C. Deser and M. Latif (1999): Pacific thermocline bridge revisited. *Geophys. Res. Lett.*, **26**, 1329–1332.

Suga, T., Y. Takei and K. Hanawa (1997): Thermostad distribution in the North Pacific Subtropical Gyre: The central mode water and the subtropical mode water. *J. Phys. Oceanogr.*, **27**, 140–152.

Williams, R. G. (1989): The influence of air-sea interaction on the ventilated thermocline. *J. Phys. Oceanogr.*, **19**, 1255–1267.

Williams, R. G., M. A. Spall and J. C. Marshall (1995): Does Stommel's mixed layer "demon" work? *J. Phys. Oceanogr.*, **25**, 3089–3102.

Xie, S.-P., T. Kunitani, A. Kubokawa, M. Nonaka and S. Hosoda (2000): Interdecadal thermocline variability in the North Pacific for 1958–1997: A GCM simulation. *J. Phys. Oceanogr.*, **30**, 2798–2813.

Yasuda, T. and K. Hanawa (1997): Decadal changes in the mode waters in the midlatitude North Pacific. *J. Phys. Oceanogr.*, **27**, 858–870.

Young, W. R. and P. B. Rhines (1982): A theory of the wind-driven circulation. II. Gyres with western boundary layers. *J. Mar. Res.*, **40**(Suppl.), 849–872.